

## Comparison of WKB and exact penetrabilities through two-peaked fission barriers

R. C. Sharma and Mario D'Amico

*Department of Physics, Concordia University, 1455 De Maisonneuve Boulevard West, Montreal, Quebec, Canada H3G 1M8*

(Received 29 June 1992)

The penetrability is computed exactly through two-peaked fission barriers consisting of three smoothly joined parabolic segments by evaluating accurately the Weber's cylinder functions appearing in the exact formulation of Cramer and Nix. When this is compared with the penetrability obtained in the WKB approximation for an identical potential barrier, it is found that the WKB transmission resonances within the intermediate well exhibit variable amounts of energy shifts from the exact resonances as large as 150 keV for narrow wells, for incident energies between the top and the bottom of the well. To illustrate the overall performance of the WKB method as an approximation to fission penetrability calculations, the ratio of penetrabilities by the WKB and the exact methods is graphically presented for all the allowed incident energies. The influence of curvature of the intermediate well, and of adjacent barriers on energy shifts is examined in detail. It is found that the use of accurate values of Weber's function yields spontaneous fission half-lives which are about 10% higher than the values reported by Cramer and Nix.

PACS number(s): 24.75.+i

### I. INTRODUCTION

Both discoveries of fission isomers and subthreshold fission [1] can be explained in terms of shell and pairing corrections introduced by Strutinsky [2]. These corrections gave a double-humped shape in the fission barrier of actinides. Most of the actinides are now known to exhibit double- or triple-humped fission barriers. Well beyond and during the past two decades, such fission barriers have generated a great deal of interest in the calculation of the probability that the nucleus will penetrate a complex barrier of this shape. To explain various fission phenomena in the actinide region, one of the methods employed by several authors to compute the probability of fission is the pioneering work of Ignatyuk, Robotnov, and Smirenkin [3], based on the traditional WKB approximation [4]. However, this approximation imposes limitations on the computation of penetrability in two ways: (1) It lacks mathematical rigor because the indiscriminate use of connection formulas at the turning points has been seriously questioned [5–11], and (2) the approximation cannot be applied for incident energies close to the top of the potential barrier and the bottom of the intermediate well.

Another successful approach, where an exact numerical solution can be obtained in terms of Weber's parabolic cylinder functions, is the case in which the multihumped barrier is composed of smoothly joined parabolic segments. Initiated by Wong and Bang [12], this technique was employed by Cramer and Nix [13] for a two-humped potential barrier (Fig. 1). In that work a comparison of exact penetrability with the calculation from the WKB formula of Ignatyuk, Robotnov, and Smirenkin [3] superficially showed that both methods produced similar results at energies well below the peaks, while increasing differences appeared in the penetrabilities at incident energies approaching the top of the bar-

rier. From the graphical representation of penetrabilities in their work [given in the inset of Fig. 2(a) of this work], it is quite clear that a close agreement seemingly exists between the penetrabilities through an asymmetric two-peaked barrier obtained by using the two methods. Subsequent to that work, these methods have been widely employed by several authors [14–21] to compute penetrability through double- or triple-humped barriers, but little attention has been given to a detailed quantitative comparison of the above methods.

The purpose of this work is to present a broad comparison of the WKB method with the exact one by computing in high precision the penetrability through a two-humped barrier constructed out of three smoothly joined parabolic segments. The precise evaluation of the Weber functions and their derivatives involved in the exact method has been successfully achieved in this work to at least eight-digit accuracy over a wide range of values of arguments. We believe that this has contributed to the significant departure of exact penetrabilities from those calculated by the WKB approximation. The probabilities computed by using the two methods are presented here and compared with the work of Cramer and Nix [13]. The differences and similarities of the results from the two methods arising with regard to symmetry of barriers, their heights, and curvature of the intermediate well are discussed in detail.

### II. CALCULATION OF PENETRABILITY AND EVALUATION OF WEBER'S FUNCTIONS

To compute the exact penetrability through the two-peaked barriers, the formula from the work of Cramer and Nix is used. Considerable effort has been involved in the precise evaluation of Weber's functions, namely,  $U(a,x)$ ,  $U(a,x)'$ ,  $V(a,x)$ ,  $V(a,x)'$ ,  $W(a,x)$ , and  $W(a,x)'$  appearing in that formula.

For negative values of  $a$  and/or  $x$ , Miller's tables [22] are reproducible for  $W(a,x)$  and  $W(a,x)'$  by the series expansion method using long double precision (10 byte number with 20-digit precision and exponential +4932). However, the series method is found to work only for small positive values of  $a$  and  $x$ . For moderate to large positive values, the most suitable method is found to be as described by Olver [23], using an Airy function calculated with Moshier's algorithm [24]. For very large values, these functions could be obtained through the use of auxiliary functions described by Fox [25]. Again, to evaluate  $U(a,x)$ ,  $V(a,x)$ , and their derivatives for small to moderate values of  $a$  and  $x$ , Moshier's algorithm for hypergeometric functions, and for large values, Oliver's method was used. The eight-digit accuracy in the evaluation of all the Weber functions was established through the use of Wronskian relations.

### III. TWO-PEAKED POTENTIAL BARRIER

Penetrabilities are computed through a two-peaked potential barrier of the type shown in Fig. 1, consisting of three smoothly joined parabolas at the connecting points  $a$  and  $b$ . The potential energy function  $V(\epsilon)$  of the system as a function of the nuclear deformation  $\epsilon$  is given by

$$\begin{aligned} V(\epsilon) &= E_1 - \frac{\mu}{2} \omega_1^2 (\epsilon - \epsilon_1)^2, \quad \epsilon \leq a \\ &= E_2 + \frac{\mu}{2} \omega_2^2 (\epsilon - \epsilon_2)^2, \quad a \leq \epsilon \\ &= E_3 - \frac{\mu}{2} \omega_3^2 (\epsilon - \epsilon_3)^2, \quad b \leq \epsilon. \end{aligned} \quad (1)$$

The energies  $E_1$  and  $E_2$  are the maximum values of the potential at the deformations  $\epsilon_1$  and  $\epsilon_3$ , respectively, and  $E$  is the minimum value at  $\epsilon_2$ .  $\mu$  is the effective mass for motion in the  $\epsilon$  direction; it is assumed to be constant for all values of  $\epsilon$ . The curvature parameters at the points  $\epsilon_1$ ,  $\epsilon_2$ , and  $\epsilon_3$ , are  $\hbar\omega_1$ ,  $\hbar\omega_2$ , and  $\hbar\omega_3$ , respectively.

The barrier defined by Eq. (1) apparently contains a total of nine parameters, three to describe each of the three parabolas. Two of the nine parameters are eliminated by the requirement that the outer parabolas join smoothly at the intersection points  $a$  and  $b$ . Another parameter can be eliminated by arbitrarily setting

$$V(\epsilon) = 0 \quad \text{at } \epsilon = 0. \quad (2)$$

TABLE I. Subthreshold fission resonances in this work (SD) and in that of Cramer and Nix (CN) for a two-peaked barrier, whose parameters are  $E_1 = 5.50$  MeV,  $\hbar\omega_1 = 1.25$  MeV,  $E_2 = 2.00$  MeV,  $\hbar\omega_2 = 1.00$  MeV,  $E_3 = 5.00$  MeV, and  $\hbar\omega_3 = 0.50$  MeV for a nuclear mass  $A = 240$ .  $P_L$  is the maximum probability selected through the best fit of the Laurentzian curve.

Level	Energy (CN) (MeV)	Energy (SD) (MeV)	$P_L$ (CN)	$P_L$ (SD)	FWHM (CN) (keV)	FWHM (SD) (keV)
$L_1$	2.492	2.4919 23	$0.699 \times 10^{-6}$	$0.69778 \times 10^{-6}$	$\approx 0.01$	$2.1 \times 10^{-5}$
$L_2$	3.430	3.4296 15	$0.349 \times 10^{-3}$	$0.34877 \times 10^{-3}$	$\approx 0.10$	$4.2 \times 10^{-3}$
$L_3$	4.215	4.2153 67	0.115	0.11440	0.196	0.195
$L_4$	4.811	4.8108 37	0.785	0.78618	9.464	9.43
Spontaneous-fission half-life	$2.45 \times 10^{12}$ yr (CN)	$2.70 \times 10^{12}$ yr (SD)				

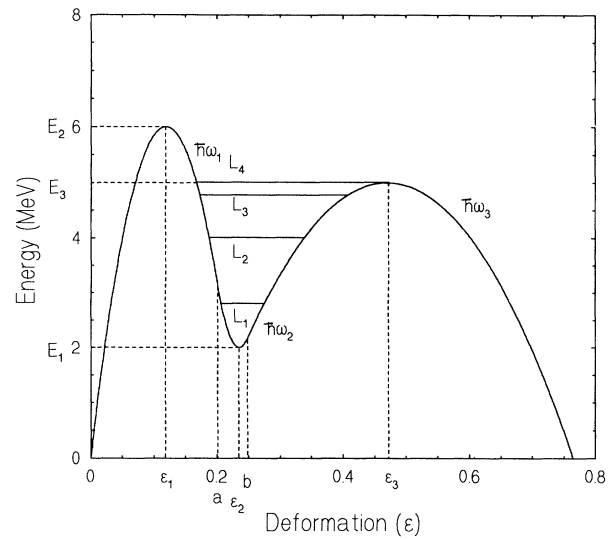


FIG. 1. Illustration of a two-peaked asymmetric fission barrier consisting of three smoothly joined parabolas. The barrier parameters are  $E_1 = 6.0$  MeV,  $\hbar\omega_1 = 1.3$  MeV,  $E_2 = 2.0$  MeV,  $\hbar\omega_2 = 2.0$  MeV,  $E_3 = 5.0$  MeV, and  $\hbar\omega_3 = 0.48$  MeV for a nuclear mass  $A = 240$ . The quasibound states  $L_1 - L_4$  in the intermediate well of the potential barrier are shown here.

This reduces the number of parameters required to define the barrier to 6. These are chosen to be the three energies  $E_1$ ,  $E_2$ , and  $E_3$  and the three curvatures  $\hbar\omega_1$ ,  $\hbar\omega_2$ , and  $\hbar\omega_3$ .

### IV. EFFECT OF ACCURACY ON EXACT PENETRABILITY

It is interesting to see whether the precise evaluation of Weber's functions appearing in the exact method makes any significant difference to the penetrability calculated previously by others. Therefore the present calculations are carried out for the same barrier parameters as used by Cramer and Nix (CN) [13] in their work. The subthreshold fission resonances and the peak values of the penetrabilities ( $P_L$ ) selected through the best-fit Laurentzian curve, from their work and ours (SD), are given in Table I. The peak values of penetrabilities for levels  $L_1$ ,  $L_2$ ,  $L_3$ , and  $L_4$  of (SD) are in very close agreement with those in

the work of (CN). Also, the energy values of the quasi-bound levels in both works agree within 0.5 keV. However, the fission widths at half maximum (FWHM) of  $L_1$  and  $L_2$  in the work of (SD) are sharply lower by factors of  $5 \times 10^{-2}$  and  $2.5 \times 10^{-1}$ , respectively, from those in the work of (CN).

## V. WKB AND EXACT PENETRABILITIES

### A. Asymmetric barrier

Penetrabilities computed by WKB and exact methods are given in Fig. 2(a) for an asymmetric potential barrier (Fig. 1). For the sake of comparison with others, the parameters of the asymmetric barrier are the same as used by (CN):  $E_1 = 6.0$  MeV,  $\hbar\omega_1 = 1.3$  MeV,  $E_2 = 2.0$  MeV,  $\hbar\omega_2 = 2.0$  MeV,  $E_3 = 5.0$  MeV, and  $\hbar\omega_3 = 0.48$  MeV. The inset of Fig. 2(a) displays the penetrability functions for the same parameters as used by (CN) using the above methods.

Figure 2(a) clearly displays the WKB penetrability resonances shifted to higher energy relative to the location of exact penetrability resonances. The magnitude of shift increases as one goes down to lower quasibound states in the intermediate well. Energy shifts, the location of WKB and exact resonances, and their respective penetrabilities at resonance are given in Table II. At 4.76 MeV peak, the energy shift in our work is 20 keV, which agrees with the value reported by (CN). However, the presence of 25 and 55.5 keV shifts at 4.0 and 2.82 MeV, respectively, has not been previously reported. Penetrability at resonance, by the exact method,  $P_m(\text{exact})$ , are in general higher than  $P_m(\text{WKB})$  by factors of 3.5, 4, and 100 at energy values of 2.82, 4.00, and 4.76 MeV, respectively. The FWHM from the WKB method for level  $L_3$  is 4.5 times larger than from the exact method.

A more explicit comparison between penetrabilities from the two methods is given in Fig. 2(b), which illustrates the semilog plot of the ratio of  $P_m(\text{WKB})$  and  $P_m(\text{exact})$  for incident energies varying from 2 to 5 MeV. The exact penetrability is accurately reproduced by the WKB method only in two short energy intervals of 3.2–3.6 and 4.3–4.5 MeV.

### B. Symmetric barrier

In Fig. 3(a) are shown the penetrabilities calculated for a symmetric potential barrier using both methods; the parameters of the barrier are the same as used by (CN):

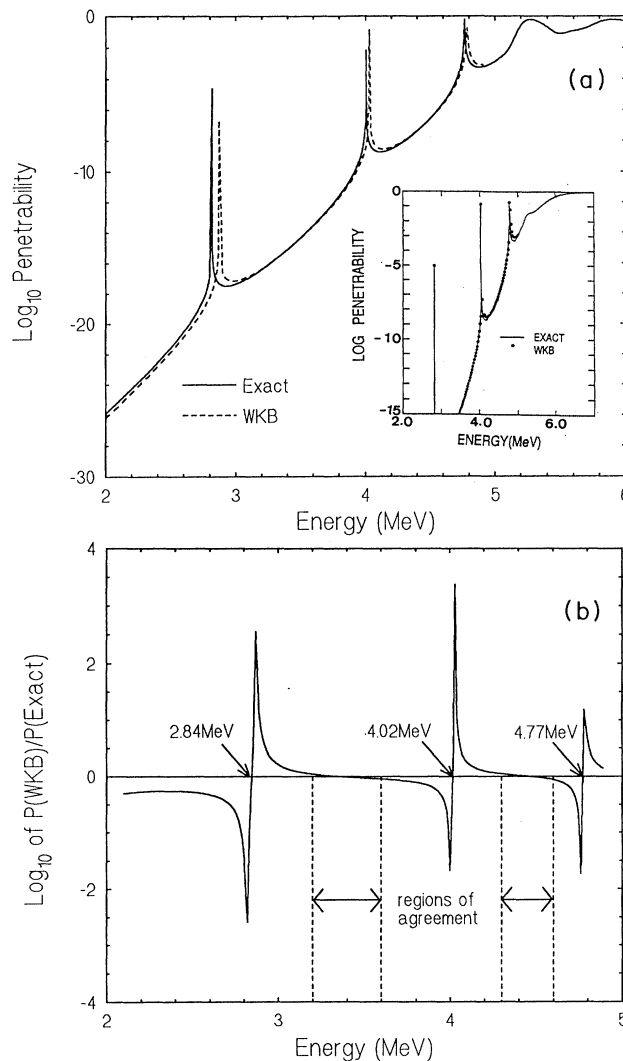


FIG. 2. Comparison of exact and WKB penetrabilities for an asymmetric barrier shown in Fig. 1 whose parameters are  $E_1 = 6.0$  MeV,  $\hbar\omega_1 = 1.3$  MeV,  $E_2 = 2.0$  MeV,  $\hbar\omega_2 = 2.0$  MeV,  $E_3 = 5.0$  MeV, and  $\hbar\omega_3 = 0.48$  MeV for a nuclear mass  $A = 240$ . (a) The semilog plot compares the exact result (solid line) and the WKB result (solid points). The increasing energy shifts between the WKB and exact methods are clearly indicated at 4.76, 4.00, and 2.82 MeV energies of resonance. The inset contains the semilog plot of penetrabilities through the same potential barrier by Cramer and Nix. (b) The semilog plot compares the WKB and exact methods in terms of the ratio of their respective penetrabilities at various incident energies.

TABLE II. WKB energy shift from exact subthreshold fission resonances for an asymmetric.

Level	$E(\text{WKB})$	$E(\text{exact})$ (MeV)	$E(\text{WKB}) - E(\text{exact})$ (keV)	$P_m(\text{WKB})$	$P_m(\text{exact})$	FWHM (WKB) (keV)	FWHM (exact) (keV)
$L_1$	2.872 496	2.816 973	55.523	$2.13 \times 10^{-7}$	$2.50 \times 10^{-5}$	$8.6 \times 10^{-5}$	$5.9 \times 10^{-5}$
$L_2$	4.029 481	4.004 371	25.110	$1.52 \times 10^{-1}$	$6.07 \times 10^{-1}$	$2.4 \times 10^{-2}$	$1.0 \times 10^{-2}$
$L_3$	4.783 384	4.763 282	20.102	$1.78 \times 10^{-1}$	$6.08 \times 10^{-1}$	$1.85 \times 10^{+1}$	4.07
Spontaneous-fission half-life		$4.61 \times 10^{11}$ yr (CN)			$5.09 \times 10^{11}$ yr (SD)		

$E_1=6.0$  MeV,  $\hbar\omega_1=1.0$  MeV,  $E_2=2.0$  MeV,  $\hbar\omega_2=0.5$  MeV,  $E_3=6.0$  MeV, and  $\hbar\omega_3=1.0$  MeV. The inset of this figure shows the penetrabilities in the work of (CN) for a symmetric barrier defined by the same parameters. The energy shift of WKB resonances from the exact ones is hardly discernible in the figure. However, contrary to the trend in the case of the asymmetric barrier, the exact penetrabilities at resonance are significantly lower than the WKB ones for the first four quasibound levels in a

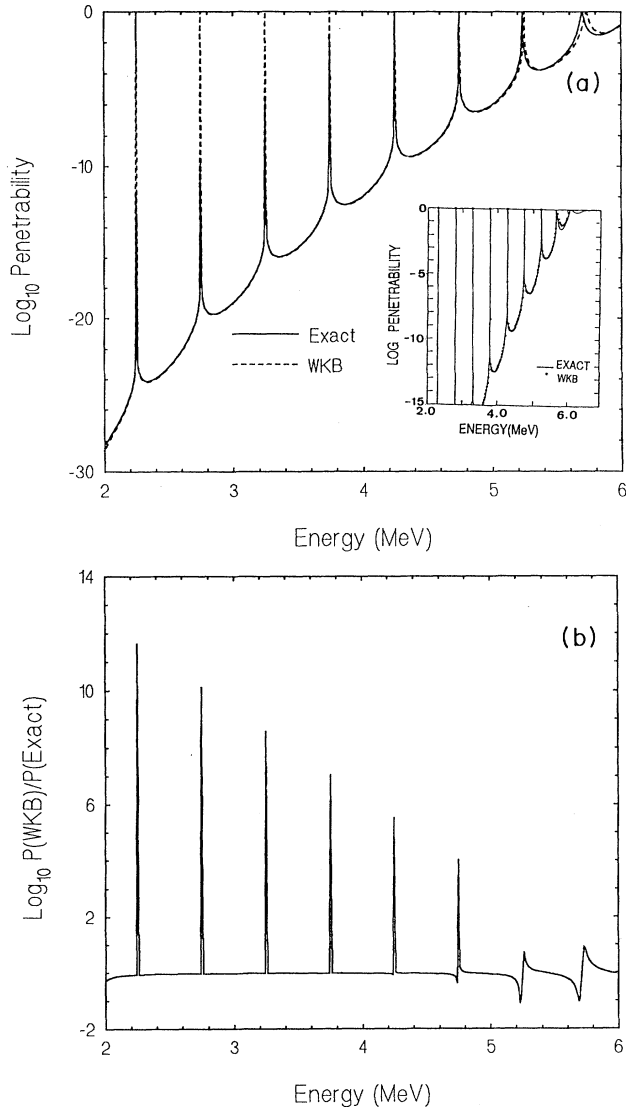


FIG. 3. Comparison of exact and WKB penetrabilities for a symmetric barrier whose parameters are  $E_1=6.0$  MeV,  $\hbar\omega_1=1.0$  MeV,  $E_2=2.0$  MeV,  $\hbar\omega_2=0.5$  MeV,  $E_3=6.0$  MeV, and  $\hbar\omega_3=0.48$  MeV for a nuclear mass  $A=240$ . (a) The semilog plot compares the exact result (solid line) and the WKB result (solid points). The inset contains the semilog plot of penetrabilities through the same potential barrier by Cramer and Nix. (b) The semilog plot compares the WKB and exact methods in term of the ratio of their respective penetrabilities at various incident energies.

symmetric barrier. A finer comparison of the two methods can be seen in Fig. 3(b), which contains a semi-log plot of the ratio of  $P_m(\text{WKB})$  to  $P_m(\text{exact})$  against the incident energy. The exact penetrabilities are accurately reproduced by the WKB method up to 5 MeV energy of incidence, except at resonance energies where the

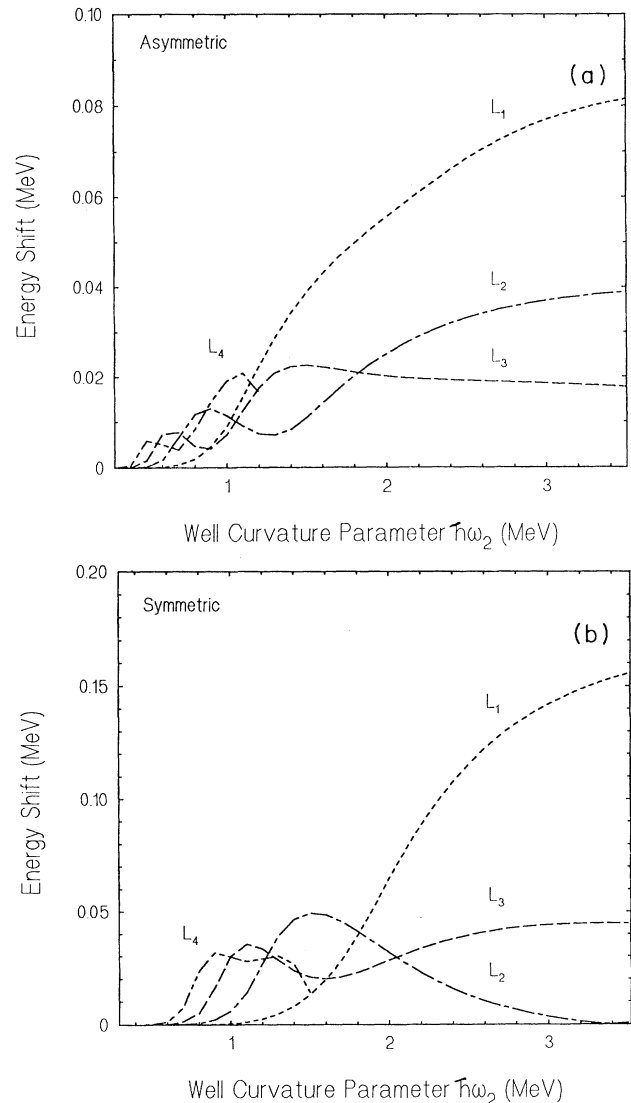


FIG. 4. Energy shift of WKB quasibound states from exact states in the intermediate well of a two-peaked potential barrier is plotted against the curvature parameter ( $\hbar\omega$ ) of the intermediate well. (a) A linear plot of the energy shift for an asymmetric barrier with the well parameter varying between 0.5 and 3.5 MeV. The fixed parameters of the barrier are  $E_1=6.0$  MeV,  $\hbar\omega_1=1.3$  MeV,  $E_2=2.0$  MeV,  $E_3=5.0$  MeV, and  $\hbar\omega_3=0.48$  MeV. Labels  $L_1, L_2$ , and  $L_3$  on the curves refer to the states in the intermediate well. (b) A linear plot of the energy shift for a symmetric barrier with the well parameter varying between 0.5 and 3.5 MeV. The fixed parameters of the barrier are  $E_1=6.0$  MeV,  $\hbar\omega_1=1.0$  MeV,  $E_2=2.0$  MeV,  $E_3=6.0$  MeV, and  $\hbar\omega_3=0.48$  MeV. The labels  $L_1, \dots, L_8$  refer to the states in the intermediate well.

TABLE III. WKB energy shift from exact subthreshold fission resonances for a symmetric two-peaked defined by the same parameters as in Fig. 3.

Level	$E(\text{WKB})$ (MeV)	$E(\text{exact})$ (MeV)	Shift (keV)	$P_m(\text{WKB})$	$P_m(\text{exact})$	FWHM(WKB) (keV)	FWHM(exact) (keV)
$L_1$	2.250 000	2.250 000	0.000	0.956	$2.18 \times 10^{-12}$	$4.9 \times 10^{-11}$	$5.0 \times 10^{-11}$
$L_2$	2.750 000	2.749 999	0.000	1.00	$1.42 \times 10^{-10}$	$9.7 \times 10^{-9}$	$9.7 \times 10^{-9}$
$L_3$	3.250 000	3.249 991	0.009	1.00	$2.44 \times 10^{-6}$	$8.7 \times 10^{-7}$	$8.8 \times 10^{-7}$
$L_4$	3.750 000	3.749 916	0.084	1.00	$1.50 \times 10^{-2}$	$4.9 \times 10^{-5}$	$5.0 \times 10^{-5}$
$L_5$	4.250 000	4.249 419	0.581	1.00	$9.03 \times 10^{-1}$	$1.9 \times 10^{-3}$	$2.0 \times 10^{-3}$
$L_6$	4.750 000	4.746 863	3.137	1.00	1.00	$6.2 \times 10^{-2}$	$6.0 \times 10^{-2}$
$L_7$	5.249 958	5.235 906	14.052	1.00	1.00	1.4	1.36
$L_8$	5.729 369	5.697 428	31.941	1.00	1.00	$2.46 \times 10^{+1}$	$2.05 \times 10^{+1}$
Spontaneous-fission half-life		$1.95 \times 10^{17}$ yr (CN)				$2.15 \times 10^{17}$ yr (SD)	

ratio of  $P_m(\text{WKB})$  to  $P_m(\text{exact})$  decreases progressively from 10 to 1 at higher levels. Energy shifts appear to be absent in the first six resonances.

In Table III are given the WKB energy shifts, the location of WKB and exact resonances, and their corresponding penetrabilities at various resonances. A shift of 31.9 keV at 5.7 MeV resonance agrees well with a 30 keV shift reported by (CN). Other unreported shifts of magnitudes 0.009, 0.084, 0.581, 3.137, and 14.052 keV appear at  $L_3, \dots, L_7$ , respectively. There is a strikingly large difference in the maximum penetrabilities for the first three resonances in the intermediate well. The

FWHM(WKB) for  $L_8$  is slightly higher than FWHM(exact).

## VI. EFFECTS OF WELL CURVATURE

It is of interest to see how energy shifts of WKB resonances from the exact ones and the maximum penetrabilities at resonances from the two methods vary with the curvature parameter ( $\hbar\omega_2$ ) of the intermediate well. Figure 4(a) displays a plot of energy shifts for various energy levels against the curvature parameter of the well of an asymmetric barrier.  $\hbar\omega_2$  is varied from 0.5 to 3.5 MeV.

TABLE IV. Energy shifts of WKB from exact resonances and their respective penetrabilities at various resonances when  $\hbar\omega_2$  is varied in increments of 0.5 MeV for an asymmetric barrier whose fixed parameters are the same as of the barrier in Fig. 1.

$\hbar\omega_2$	0.40	0.90	1.40	1.90	2.40	2.90	3.40
$P_m(\text{exact})$	$2.829\ 68 \times 10^{-19}$	$3.201\ 19 \times 10^{-10}$	$2.308\ 36 \times 10^{-06}$	$8.764\ 78 \times 10^{-05}$	$2.715\ 75 \times 10^{-04}$	$3.279\ 11 \times 10^{-04}$	$1.211\ 23 \times 10^{-01}$
$L_1 P_m(\text{WKB})$	$2.159\ 02 \times 10^{-12}$	$1.645\ 70 \times 10^{-06}$	$5.128\ 04 \times 10^{-08}$	$2.966\ 98 \times 10^{-08}$	$5.554\ 36 \times 10^{-07}$	$1.136\ 04 \times 10^{-06}$	$3.713\ 95 \times 10^{-06}$
$E(\text{shift})$	0.000 000 00	0.004 522 09	0.034 058 09	0.052 733 90	0.065 943 00	0.080 817 94	0.075 633 05
$P_m(\text{exact})$	$8.150\ 22 \times 10^{-13}$	$1.213\ 82 \times 10^{-01}$	$5.131\ 07 \times 10^{-01}$	$6.059\ 59 \times 10^{-01}$	$6.071\ 40 \times 10^{-01}$	$6.076\ 42 \times 10^{-01}$	$6.062\ 69 \times 10^{-01}$
$L_2 P_m(\text{WKB})$	$5.283\ 06 \times 10^{-04}$	$5.057\ 49 \times 10^{-05}$	$1.775\ 62 \times 10^{-02}$	$1.207\ 26 \times 10^{-01}$	$2.967\ 53 \times 10^{-01}$	$4.644\ 87 \times 10^{-01}$	$5.908\ 93 \times 10^{-01}$
$E(\text{shift})$	0.000 006 91	0.012 866 97	0.008 260 97	0.022 766 11	0.031 872 27	0.036 345 01	0.038 578 03
$P_m(\text{exact})$	$4.511\ 84 \times 10^{-10}$	$6.038\ 94 \times 10^{-01}$	$6.076\ 41 \times 10^{-01}$	$6.076\ 44 \times 10^{-01}$			
$L_3 P_m(\text{WKB})$	$3.783\ 53 \times 10^{-03}$	$2.223\ 31 \times 10^{-01}$	$7.085\ 26 \times 10^{-01}$	$2.107\ 80 \times 10^{-01}$	$1.099\ 15 \times 10^{-01}$	$7.931\ 56 \times 10^{-02}$	$6.649\ 58 \times 10^{-02}$
$E(\text{shift})$	0.000 077 01	0.004 095 08	0.022 255 90	0.020 519 26	0.019 233 23	0.018 626 21	0.017 849 92
$P_m(\text{exact})$	$1.266\ 95 \times 10^{-05}$	$6.076\ 43 \times 10^{-01}$					
$L_4 P_m(\text{WKB})$	$2.847\ 27 \times 10^{-02}$	$3.395\ 01 \times 10^{-01}$					
$E(\text{shift})$	0.000 543 12	0.0143 399 2					
$P_m(\text{exact})$	$5.470\ 26 \times 10^{-01}$						
$L_5 P_m(\text{WKB})$	$8.975\ 65 \times 10^{-03}$						
$E(\text{shift})$	0.002 727 03						
$P_m(\text{exact})$	$5.979\ 17 \times 10^{-01}$						
$L_6 P_m(\text{WKB})$	$9.493\ 18 \times 10^{-01}$						
$E(\text{shift})$	0.005 201 34						
$P_m(\text{exact})$	$6.076\ 31 \times 10^{-01}$						
$L_7 P_m(\text{WKB})$	$4.200\ 18 \times 10^{-01}$						
$E(\text{shift})$	0.004 644 87						
$P_m(\text{exact})$	$6.076\ 44 \times 10^{-01}$						
$L_8 P_m(\text{WKB})$	$5.486\ 14 \times 10^{-02}$						
$E(\text{shift})$	0.007 956 03						



by the WKB approximation for energies well below the barrier tops, as illustrated for an asymmetric barrier in Fig. 2(a), its inset depicting the results by CN for visual comparison with this work. The increasing forward shift in energy of the WKB peaks from the exact ones for incident energy near the well bottom is particularly striking. As a consequence of these shifts, as shown in Fig. 2(b), the logarithm of the ratio  $P_m(\text{WKB})/P_m(\text{exact})$  ex-

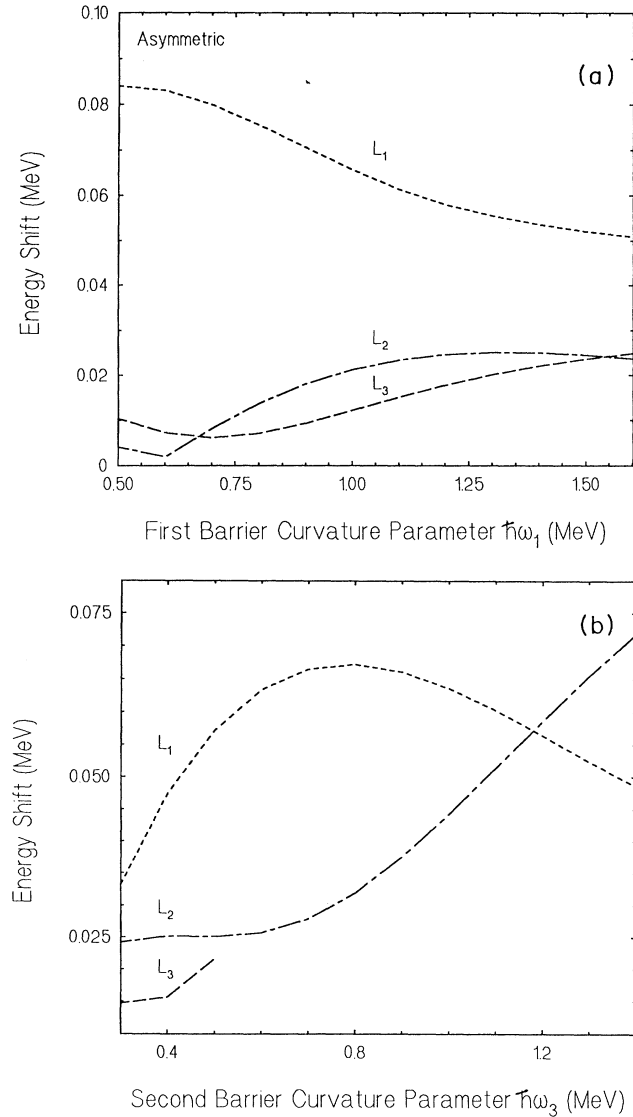


FIG. 5. Energy shift of WKB quasibound states from exact states in the intermediate well of a two-peaked potential barrier is plotted against the curvature parameter of the two barriers. (a) A linear plot of the energy shift for an asymmetric barrier with the first barrier parameter  $\hbar\omega$ , varying between 0.5 and 1.5 MeV. The fixed parameters are  $E_1 = 6.0$  MeV,  $E_2 = 2.0$  MeV,  $\hbar\omega = 2.0$  MeV,  $E_3 = 5.0$  MeV, and  $\hbar\omega_3 = 0.48$  MeV. Labels  $L_1$ ,  $L_2$ , and  $L_3$  on the curves refer to the states in the intermediate well. (b) A linear plot of the energy shift for the same asymmetric barrier as in (a) with the second barrier parameter  $\hbar\omega$  varying between 0.5 and 1.5 MeV.

hibits a sudden jump in magnitude about the peak positions within a very narrow energy width depending on the size of the shift. The WKB method reproduces the exact penetrabilities in only two narrow energy intervals, marked by dotted lines in the Fig. 2. It should also be noted in Table II that the maximum penetrability ( $P_m$ ) at the lowest resonance by the exact method is about 100 times higher than that given by the WKB method, besides a 55.5 keV energy shift. The FWHM(exact) for the three levels in the intermediate well are lower than the corresponding FWHM(WKB), the difference in fission width from the two methods increasing with higher energy levels.

Looking into the penetrability functions of Figs. 3(a) and 3(b) for a symmetric barrier, a slightly different picture seems to emerge. There are hardly any noticeable energy shifts in the first six resonances, and the exact penetrabilities are accurately reproduced by the WKB method in the regions between the peaks. This is quite consistent with the results of CN given in the inset of Fig. 3(a). However, from Table III,  $P_m$ 's by the WKB method are sharply higher than the exact ones for the three lower resonances, and FWHM(WKB) for  $L_8$  is about 4 keV higher than FWHM(exact).

It was deemed essential to investigate the effects of variation of the well-curvature parameter on energy shifts and  $P_m$ 's using the two methods. The results of such computation are summarized in Tables IV and V for asymmetric and symmetric barriers, respectively. The linear plots of the energy shift versus curvature for the two types of barriers are displayed in Figs. 4(a) and 4(b). From Fig. 4(a) and Table IV concerning an asymmetric barrier, it is clear that the energy shifts of the three lowest levels in the well are small ( $\sim 7.5$  KeV) for 1 MeV curvature; shifts of  $L_1$  and  $L_2$  reach 80 and 39 keV, respectively, at curvatures between 1 and 3 MeV, while  $L_3$  reaches a 20 keV plateau around 1.5 MeV. Moreover, there is a crossover of  $L_2$  and  $L_3$  shifts around 1.75 MeV.

The energy shifts of the three lowest levels in the well of a symmetric barrier [Fig. 4(b) and Table V] exhibit a slightly different trend from the case of an asymmetric barrier. The shift function of  $L_1$  is zero below 1 MeV and then rises to a 150 keV plateau between 1 and 3.25 MeV curvature. The  $L_2$  function starts rising from zero at 0.8 MeV to a maximum of a 49 keV shift at 1.5 MeV, and then decreases to zero again at 3.25 MeV curvature.  $L_3$  starts rising at 0.7 MeV, attains a peak value of 30 keV at 1 MeV, decreases to a minimum at 1.6 MeV, and starts rising again to a 45 keV plateau at 3.5 MeV. The shift functions of  $L_1$  and  $L_2$  intersect twice at 1.2 and 2 MeV curvatures.

In the course of this study, comparison of penetrability through a single barrier using the two methods was carried out. The WKB method reproduced the exact penetrability quite accurately in most of the energy range, with only slight deviations occurring at the lower end of incident energy. The lifetime of a spontaneously fissioning isomer depends upon the penetrability through each of the two peaks surrounding the secondary minimum. Consequently, both are expected to yield the same results for the half-life of a spontaneously fissioning isomer.

The spontaneous-fission half-life for a nucleus was determined by computing the zero-energy penetrability using the exact method and substituting into the equation [13]

$$T_0^{\text{sf}} = 10^{-28} [P(E_0)]^{-1} \text{ yr} , \quad (3)$$

for an estimated first-well curvature of 1 MeV. As given in Tables I–III, the spontaneous-fission half-lives in our work are 10% higher than the values obtained by CN.

### IX. CONCLUSION

In this work a detailed comparison of exact penetrabilities with those from the WKB approximation for both symmetric and asymmetric two-humped barriers reveals more pronounced differences than previously reported, as a consequence of the precise evaluation of Weber's functions appearing in the exact method. While strongly dependent on the well-curvature parameter, the WKB penetrability resonances exhibit forward energy shifts from the exact ones, ranging between 0 and 150 keV for the data used in this work. Generally, the magnitude of this shift tends to be greater for incident energies near the bottom of the well, rather than near the top.

The maximum penetrabilities at resonance computed by the exact method are generally smaller than the ones

obtained by using the WKB approximation. For some low-lying resonances in the intermediate well, the exact penetrabilities are found to be lower, as much as by a factor of  $10^{-12}$ . The FWHM's given by the exact method are considerably smaller than those by the WKB method for energy levels near the top of the intermediate well, which is an important region of incident energy where the fission cross-section data are widely available.

It has been found fruitful to evaluate Weber's functions accurately when using the exact method to compute penetrability through two-humped barriers. The spontaneous-fission half-lives obtained for such types of barriers in this work by using the exact method are about 10% higher than the ones by CN of the same parameters.

Finally, it may be noted that the exact method is applicable to potential barriers consisting of smoothly joined parabolic segments. There are no strong reasons to believe that the shape of the barrier remains quadratic for all deformations during the fission process. As a matter of fact, there exists a large uncertainty as to the exact shape of the potential barrier.

### ACKNOWLEDGMENTS

We would like to thank Joseph Shin for his useful suggestions regarding this study.

- 
- [1] *Advances in Nuclear Physics*, edited by A. Michaudon, M. Baranger, and E. Vogt (Plenum, New York, 1973), Vol. 6.
- [2] V. M. Strutinsky, *Nucl. Phys.* **A95**, 420 (1967).
- [3] A. V. Ignatyuk, N. S. Robotnov, and V. M. Smirenkin, *Phys. Lett.* **29B**, 209 (1969).
- [4] D. Bohm, *Quantum Theory* (Prentice-Hall, Englewood Cliffs, NJ) (1961).
- [5] F. W. J. Oliver, *Philos. Trans. R. Soc. London A* **247**, 307 (1955).
- [6] J. Heading, *Proc. Cambridge Philos. Soc.* **52**, 399 (1957).
- [7] F. W. J. Oliver, *Philos. Trans. R. Soc. London A* **250**, 479 (1958).
- [8] A. Messiah, *Quantum Mechanics* (North-Holland, Amsterdam, 1958), Vol. 1, p. 236.
- [9] E. Merzbacher, *Quantum Mechanics* (Wiley, New York, 1961), p. 112.
- [10] N. Froman and O. Froman, *JWKB Approximation* (North-Holland, Amsterdam, 1965).
- [11] J. N. Leboeuf and R. C. Sharma, *Can. J. Phys.* **51**, 446 (1973).
- [12] C. Y. Wong and J. Bang, *Phys. Lett.* **29B**, 143 (1969).
- [13] J. D. Cramer and J. R. Nix, *Phys. Rev. C* **2**, 1048 (1970).
- [14] R. C. Sharma and J. N. Leboeuf, *Phys. Rev. C* **11**, 1849 (1975).
- [15] R. C. Sharma and J. N. Leboeuf, *Phys. Rev. C* **14**, 2340 (1976).
- [16] M. Prakash, *J. Phys. A* **9**, 1847 (1976).
- [17] M. Prakash and B. S. Bhandari, *Phys. Rev. C* **18**, 1531 (1977).
- [18] M. Prakash, *J. Phys. G* **4**, 1455 (1978).
- [19] B. S. Bhandari, *Phys. Rev. C* **19**, 1820 (1979).
- [20] B. S. Bhandari, *Phys. Rev. C* **22**, 606 (1980).
- [21] B. S. Bhandari and A. S. Al-Kharam, *Phys. Rev. C* **39**, 917 (1989).
- [22] J. C. P. Miller, *Tables of Weber Parabolic Cylinder Functions* (Her Majesty's Stationery Office, London, 1955).
- [23] F. W. Oliver, *J. Res. Natl. Bur. Stand.* **63B**, 131 (1959).
- [24] S. L. Moshier, *Methods and Programs for Mathematical Functions* (Wiley, New York, 1989).
- [25] L. Fox, *Tables of Weber Parabolic Cylinder Functions and Other Functions for Large Arguments* (Her Majesty's Stationery Office, London, 1960).